An Examination of the Shear-Thickening Behavior of High Molecular Weight Polymers Dissolved in Low-Viscosity Newtonian Solvents

B. J. EDWARDS, D. J. KEFFER, C. W. RENEAU

Department of Chemical Engineering, University of Tennessee, Knoxville, Tennessee 37996

Received 1 June 2001; accepted 14 November 2001

ABSTRACT: The anomaly of shear thickening at high shear rates can be observed under certain conditions for high molecular weight polymers dissolved in low-viscosity Newtonian solvents despite the fact that shear-thinning behavior is considered the norm for these fluids. The nature of the shear-thickening region of the flow curve is examined herein through the application of a recent rheological model that has the capability of quantifying not only the rheological properties of the material, but its internal microstructural state as well. The results of this examination provide a self-consistent explanation of the full flow characterization of this anomalous behavior, including both rheological and optical experimental measurements. The results presented herein suggest that the shear-thickening behavior is actually caused by the destruction of structures formed during shear at lower shear rates, not by their formation, as previously assumed. The linear birefringence and linear dichroism observed experimentally in correlation with the shear-thickening behavior are well described by the rheological model and give predictions in line with experimental measurements. Furthermore, quantitative predictions are made for rheological characteristic functions, such as the first and second normal-stress coefficients, for which experimental measurements for these solutions have not yet been made. © 2002 Wiley Periodicals, Inc. J Appl Polym Sci 85: 1714–1735, 2002

Key words: dilute solutions; flow-induced phase separation; shear thickening; rheo-optical properties

INTRODUCTION

". . . future work in this area should concentrate on the prediction of the relationship between shear-thickening and structure formation from a first principles model. The above explanation, while consistent, is an amalgamation of experimental observations and theories or approximations. While all evidence supports the conclusions drawn from the rheo-optical study, a single theory that could predict both the rheology and the optical behavior simultaneously would characterize the nature of the structure formation more precisely. A successful single theory would also lead to the possible prediction of new phenomena to be investigated experimentally."[1]

The passage quoted above is the final paragraph of the dissertation of A. J. Kishbaugh, University of Illinois, 1992.[1] This work, published by Kishbaugh and McHugh,[2,3] finally established a clear connection between the anomalous pattern of shear thickening, which occurs under high shear conditions in several dilute polymer solutions, and the shear-induced structure formation in the same. Although this connection had been

Correspondence to: B. J. Edwards (bjedwards@chem.engr.utk.edu).

Journal of Applied Polymer Science, Vol. 85, 1714–1735 (2002)

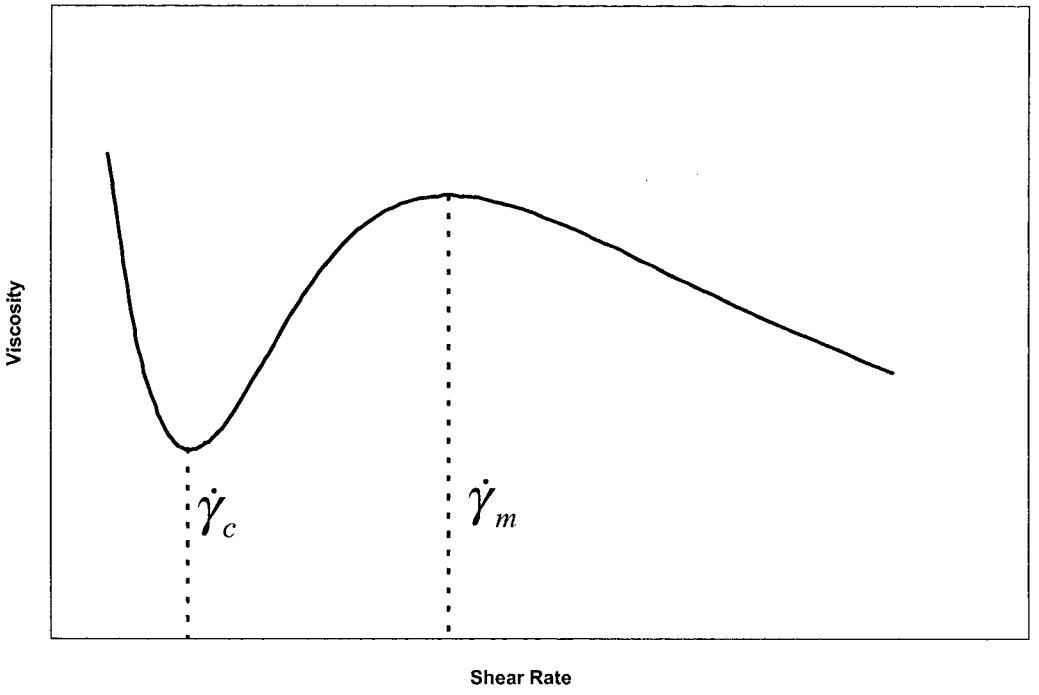

Figure 1 A typical plot of viscosity versus shear rate for a dilute polymer solution that exhibits shear thickening. The increase in viscosity begins at the critical shear rate $\dot{\gamma}_c$, and shear thinning resumes at $\dot{\gamma}_m$.

clearly established in refs. 1–3, the authors recognized that no rheological theory had yet been developed that could self-consistently describe all of the phenomena observed in the experimental investigation, let alone be used to predict associated phenomena that had not yet been observed experimentally. In this article, we demonstrate that this statement is no longer true. The two-coupled Maxwell modes (TCMM) model, developed in ref. 4 and analyzed extensively in ref. 5, is shown to give quantitative descriptions of all aspects associated with the shear-thickening behavior of these solutions, as well as predictions for other viscometric properties that have not heretofore been measured experimentally.

Before we continue, let us first explain the phenomenon under consideration. Dilute solutions of high molecular weight polymers dissolved in low-viscosity, Newtonian solvents are expected to exhibit purely shear-thinning behavior at intermediate and high shear rates (i.e., the viscosity of the solution decreases with increasing shear rate). However, an anomalous behavior was noted on some occasions, for many years now, which is still not widely accepted. This anomalous behavior is termed shear-thickening, and it manifests as the opposite effect to shear thinning: the viscosity of the solution increases with increasing shear rate.[6,7] Although the shear-thinning phenomenon is widely understood and accepted as an intramolecular effect occurring because of the extension and orientation of the polymer chains in solution,[8] prior to the past decade, no consensus had arisen to explain the origin of shear thickening. Some minds even questioned whether it existed at all in this kind of solution, preferring to believe that it was caused by some other well-known but not well-quantified phenomenon such as viscous heating, polymer adsorption on walls, or capillary entrance effects. The work of Kishbaugh and McHugh,[2,3] as mentioned above, has finally established the clear connection of this unusual viscosity pattern with intermolecular effects, not to mention establishing further documentation as to its mere existence.

A typical flow curve for a dilute solution undergoing steady shear flow is presented in Figure 1. This figure shows the experimental behavior observed with increasing shear rate, as observed by Layec-Raphalen and Wolff[6] and Vrahopoulou and McHugh.[7] At low to intermediate shear rates (following the common Newtonian plateau for very small shear rates), one observes the usual pattern of shear thinning with increasing shear rate.

However, as the shear rate continues to increase, a critical shear rate is attained where the viscosity reaches a local minimum at $\dot{\gamma}_c$ and actually begins increasing with increasing shear rate thereafter. At very high shear rates, a local maximum in the viscosity is achieved at $\dot{\gamma}_m$, and a weak plateau and subsequent shear-thinning region follow at extremely high shear rates.

Various explanations were advanced over the years to rationalize this observed behavior. Some of these were intramolecular,[9–12] and some were intermolecular[13–16]; however, we omit a review of these, because all of them were demonstrated as inapplicable to the solutions under consideration by the experimental results of Kishbaugh and McHugh[2] (see below). Still, on the basis of the trends observed in Figure 1, Vrahopoulou and McHugh[7] offered a rational intermolecular explanation for this behavior, which eventually evolved into the more sophisticated explanation of Kishbaugh and McHugh.[2,3] In the explanation of the former authors,[7] experimental curves, such as the one displayed in Figure 1, arise as follows. Initially, at low to moderate shear rates, the typical flow behavior of a dilute polymer solution is observed, indicating the intramolecular chain stretching and orientation of the polymer molecules subject to hydrodynamic interactions only. However, at a critical shear rate, $\dot{\gamma}_c$, intermolecular associations begin to develop which produce amorphous structures that can be much larger than the average chain dimensions. These structures grow in size with increasing shear rate, thus raising the solution viscosity. At some higher critical shear rate ($\dot{\gamma}_m$), however, the magnitude of the imposed shear becomes so severe that the formed structures are sheared apart, thus producing the second region of shear-thinning behavior at extremely high shear rates. Still, as long as only rheological experiments were conducted, no conclusive evidence could be amassed to prove the existence of a shear-thickening/structure-formation region in the flow curves of these solutions: at the high shear rates involved, a skeptic could always argue that the observed increase in viscosity was actually caused by some phenomenon unrelated to the structure formation, such as polymer adsorption on the walls of the rheometer.

Definitive experimental evidence confirming the intermolecular nature of shear thickening was provided in 1992 by Kishbaugh and McHugh.[1,2] In these experiments, *in situ* optical measurements of the linear dichroism and linear birefringence, the imaginary and real parts of the difference between principal indexes of the refractive index tensor, were made simultaneously with measurements of the viscosity. The shear thickening behavior was observed to begin at a critical shear rate that was typically slightly larger than or equal to the shear rate where the linear dichroism displayed a global maximum, $\dot{\gamma}_d$ (see Fig. 2). At the same time, the linear birefringence increased monotonically with increasing shear rate.

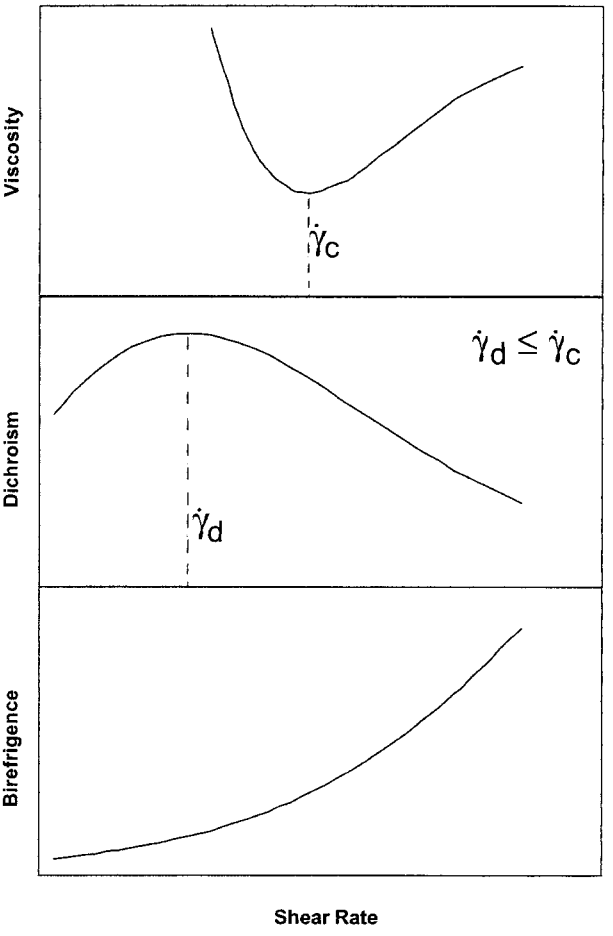

Figure 2 Typical flow curves for viscosity, dichroism, and birefringence versus shear rate as observed in simultaneous rheo-optical measurements. Note that $\dot{\gamma}_d \leq \dot{\gamma}_c$.

On the basis of these experimental findings, Kishbaugh and McHugh[3] advanced a sounder conceptual basis for the observed shear-thickening behavior, which refines the explanation developed by Vrahopoulou and McHugh.[7] Before the critical shear rate where the shear-thickening behavior manifests, the solutions begin to develop micron-size, optically isotropic particles composed of associated polymer chains, which orient along the flow direction. These particles grow in size

with increasing shear rate, and, according to the anomalous diffraction approximation (ADA) light scattering theory, this causes the maximum in the linear dichroism curve.[3] However, most polymer chains remain in the solution, not in the particles, and it is the extension and orientation of these that cause the monotonic increase in the linear birefringence with increasing shear rate.

In this article, we shall show that, according to the TCMM model, the above explanation may not be totally correct. In the above explanation, there is really no reason the onset of shear thickening must always occur at an equal or slightly larger value of the shear rate than the maximum in dichroism curve. If amorphous particles are forming and enlarging in the polymer solution over a range of shear rates spanning the viscosity minimum, then it can be nothing more than coincidence that the maxima in the dichroic curves always correlate with the minima in the viscosity curves (see below). However, according to the TCMM model, as shown below, the particles (associations of polymers) actually grow at shear rates well below the viscosity minimum. These structures cause the rise in the dichroic curve up to the maximum values, and actually augment the shear-thinning behavior (i.e., they lower the effective shear stress by relieving some of the forces acting on the anisotropic polymer chains in the bulk flow). At the critical shear rate of the dichroic maximum, these structures begin to decrease in size and aspect ratio because of the strong hydrodynamic forces, thus raising the shear stress and increasing the effective viscosity, while causing the dichroic signal to begin retracing its path backward as the effective particle size decreases. This provides a rational explanation as to why the viscosity minima and dichroic maxima always occur at approximately the same shear rates, whereas the explanation in ref. 3 does not.

Another criticism of the Kishbaugh and McHugh hypothesis is that the size of the particles (on the order of microns) seems rather large. If such large amorphous structures are forming, then polymer molecules are being subtracted from the optically active bulk fluid to form them; however, the solution birefringence shows no sign of this occurrence as it continues to increase exponentially with increasing shear rate. According to the TCMM model, the particles are actually two orders of magnitude smaller, but more numerous than in the Kishbaugh and McHugh hypothesis. Consequently, their dichroic behavior can be described well by the Rayleigh scattering theory, as demonstrated below. However, the above-stated criticism is not overcome in this manner. To overcome it, we must envision these structures not as separate entities composed of amorphous polymer molecules, but rather as an interpenetrating structured continuum imposed over the bulk chains in solution. Therefore, the structures themselves may not be optically isotropic, as previously believed.[2,3] Interestingly, the results presented below can be used to understand the physics of the precursor state to flow-induced phase separation in polymer solutions of higher concentration. Furthermore, by fitting the parameters in the TCMM model against the experimental data from the literature, predictions are obtained for characteristic functions and optical properties that have yet to be measured experimentally for these solutions.

THE TCMM MODEL

The TCMM model was developed by using the thermodynamic methodology put forth over the past decade by Beris and Edwards[4] and Grmela and Öttinger.[17,18] It first appeared in multiple mode form in ref. 4, and the two-mode version was analyzed extensively in ref. 5, wherein it was shown that this model was able to reproduce the complex qualitative behavior that is typically ascribed to polymeric liquids. This model is written in terms of two mode-conformation tensors, $\mathbf{c}^1$ and $\mathbf{c}^2$, one for each relaxation mode of the polymeric liquid. Although most polymeric fluids possess a whole spectrum of relaxation times, the qualitative behavior of both the linear and the nonlinear rheological properties can be adequately described with just two modes.[5] For dilute polymer solutions, two modes should allow ample latitude to obtain reasonably good quantitative fits to the experimental data of interest.

The two relaxation modes give a direct quantification of the microstructural state of the polymeric fluid. The eigenvalues and eigenvectors of these second-rank tensors quantify the degree of orientation and its preferred direction, respectively, corresponding to the two relaxation modes. For the present case, $\mathbf{c}^1(\mathbf{x}, t)$ is taken as the second moment of the orientational distribution function, $\psi(\mathbf{x}, \mathbf{R}, t)$[8]:

$$\mathbf{c}^1 = \int \mathbf{R}\mathbf{R}\psi d^3R \tag{1}$$

In this expression, $\mathbf{R}$ is the end-to-end vector of a dissolved polymer chain, and $\mathbf{c}^1$ thus has units of length squared.

The second mode tensor, $\mathbf{c}^2(\mathbf{x}, t)$, is associated with the intermolecular structures that form during shear. It, too, is correlated with the size of the structures formed. If we define a size distribution function by $f(\mathbf{x}, \mathbf{a}, t)$, where $\mathbf{a}$ is the vector spanning the major axis of a spheroidal structure, then

$$\mathbf{c}^2 = \int \mathbf{aa} f d^3a \tag{2}$$

The fundamental tenet of the TCMM model is that these two mode-conformation tensors are not only affected by the imposed deformation, but also by each other.[4] A typical differential rheological model involves uncoupled modes, in which the individual mode tensors are affected by the imposed deformation only. Within the auspices of the generalized bracket approach to thermodynamic modeling, a general class of coupled relaxation-mode models was derived.[4] In the two-mode limit, the evolution equations for the mode-conformation tensors are

$$\frac{\partial c^1_{\alpha\beta}}{\partial t} + \nu_\gamma \nabla_\gamma c^1_{\alpha\beta} - c^1_{\alpha\gamma}\nabla_\gamma \nu_\beta - c^1_{\beta_\gamma}\nabla_\gamma \nu_\alpha = -\frac{1}{\lambda_1} c^1_{\alpha\beta} + \frac{k_B T}{\lambda_1 K_1}\delta_{\alpha\beta} - \frac{\theta}{2k_B T}\sqrt{\frac{n_2}{n_1}}\frac{1}{\sqrt{\lambda_1\lambda_2}}[K_2(c^1_{\alpha\gamma}c^2_{\beta_\gamma} + c^2_{\alpha\gamma}c^1_{\beta_\gamma}) - 2k_B T c^1_{\alpha\beta}]$$

$$\frac{\partial c^2_{\alpha\beta}}{\partial t} + \nu_\gamma \nabla_\gamma c^2_{\alpha\beta} - c^2_{\alpha\gamma}\nabla_\gamma \nu_\beta - c^2_{\beta_\gamma}\nabla_\gamma \nu_\alpha = -\frac{1}{\lambda_2} c^2_{\alpha\beta} + \frac{k_B T}{\lambda_2 K_2}\delta_{\alpha\beta} - \frac{\theta}{2k_B T}\sqrt{\frac{n_2}{n_1}}\frac{1}{\sqrt{\lambda_1\lambda_2}} \times [K_1(c^1_{\alpha\gamma}c^2_{\beta_\gamma} + c^2_{\alpha\gamma}c^1_{\beta_\gamma}) - 2k_B T c^2_{\alpha\beta}] \tag{3}$$

In the present context, the polymer associations quantified by $\mathbf{c}^2$ are assumed to possess the same type of elasticity as the individual chains (i.e., Maxwellian), but this elasticity acts over much larger length and time scales.

In the above expressions, five adjustable parameters appear in addition to Boltzmann's constant, k_B, the absolute temperature, T, and the Hookean spring constants, K_1 and K_2. These are λ_1, λ_2, n_1, n_2, and θ. The first two are the constant relaxation times of the two modes, measured in units of time. The second two are the effective concentrations of the two modes, measured in units of moles per volume. All four of these parameters must be greater than or equal to zero for the model to make sense physically. The last parameter quantifies the degree of interaction between the two modes. Thermodynamically, this parameter should be within the range of $-1 \leq \theta \leq 1$; however, as noted in ref. 5, θ is typically a small positive fraction.

The extra stress tensor used for calculating the rheological properties of the polymer solutions is a linear sum over the mode-conformation tensors:

$$\sigma_{\alpha\beta} = \sum_{i=1}^{2} (n_i N_A K_i c^i_{\alpha\beta} - n_i N_A k_B T \delta_{\alpha\beta}) \tag{4}$$

where N_A is Avogadro's number. It has units of force per length squared, and the shear viscosity, η, is calculated by dividing the shear stress component, σ_{12}, by the shear rate, $\dot{\gamma}$. Other rheological characteristic functions and optical properties will be defined where appropriate.

GENERAL BEHAVIOR OF THE TCMM MODEL IN STEADY SHEAR FLOW

The general behavior of the TCMM model in steady shear flow was already examined in ref. 5; however, no special attention was paid there to the parameter region at high shear rates where the phenomenon of shear thickening may occur. Here, we examine more closely the high shear rate region of the flow curve, for varying parameter ranges, to see what effects mode coupling has upon not only the shear viscosity of the polymeric solutions, but also their other rheological characteristic functions. To do this more efficiently, we work in terms of dimensionless quantities.

The evolution equations, eq. (3), are made dimensionless by defining the dimensionless shear rate as $\tilde{\gamma} \equiv \dot{\gamma}\sqrt{\lambda_1\lambda_2}$, the dimensionless mode tensors as $\tilde{c}^i_{\alpha\beta} \equiv K_i c^i_{\alpha\beta}/k_B T$, and dimensionless time as $\tilde{t} \equiv t/\sqrt{\lambda_1\lambda_2}$. For a specified value of the shear rate, these coupled, nonlinear algebraic equations are solved via Newton's method, and the dimensionless shear stress is computed according to $\tilde{\sigma}_{12} \equiv \sigma_{12}/\sqrt{n_1 n_2}\, k_B T$. Hence, the dimensionless viscosity is given by $\tilde{\eta} \equiv \tilde{\sigma}_{12}/\tilde{\gamma}$. Furthermore, the first and second normal stress

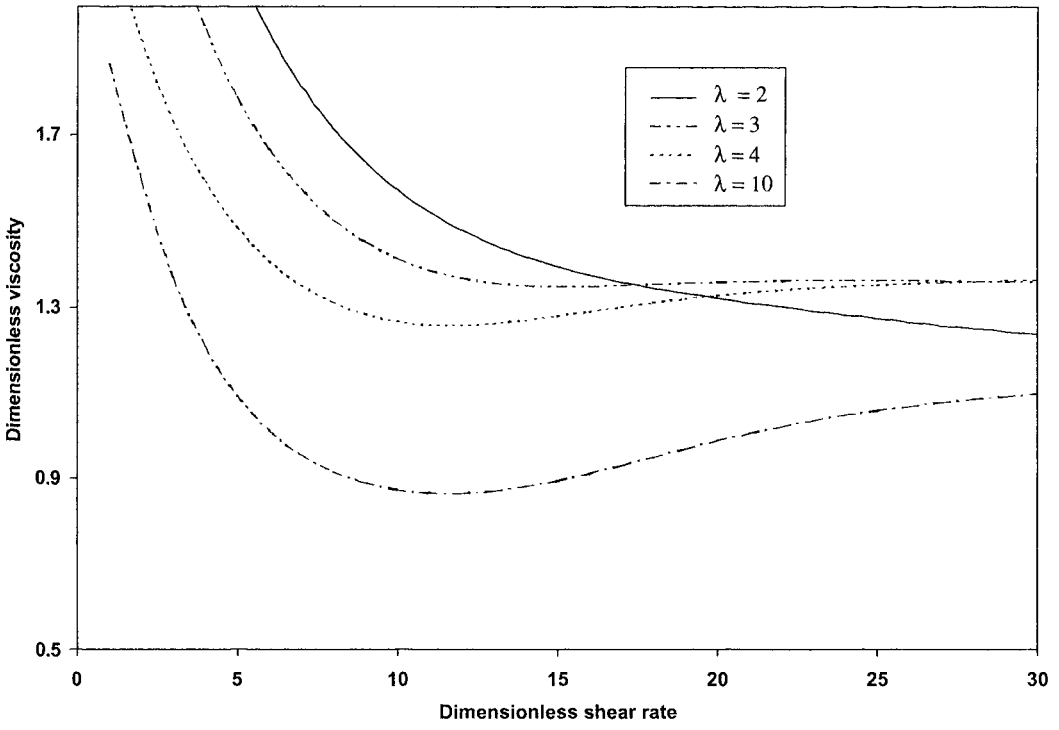

Figure 3 Dimensionless flow curves for $n = 0.05$, $\theta = 0.1$, and various values of λ.

coefficients, in dimensionless forms, are given by $\tilde{\Psi}_1 \equiv (\tilde{\sigma}_{11} - \tilde{\sigma}_{22})/\tilde{\gamma}^2$ and $\tilde{\Psi}_2 \equiv (\tilde{\sigma}_{22} - \tilde{\sigma}_{33})/\tilde{\gamma}^2$. When expressed in dimensionless form, the dependence of the evolution equations, eq. (3), reduces to three parameters, the ratio of the mode relaxation times, $\lambda \equiv \lambda_2/\lambda_1$, the ratio of the mode concentrations, $n \equiv n_2/n_1$, and the coupling parameter, θ.

Figure 3 plots the results of calculations for the dimensionless viscosity versus dimensionless shear rate for $n = 0.05$, $\theta = 0.1$, and various values of λ. This demonstrates that the TCMM model is well capable of describing the qualitative behavior of the experimental data for these solutions. For values of λ less than approximately 3, the behavior is the expected shear thinning with a saturation at high values of the shear rate. For λ values between approximately 3 and 100, one finds a region of shear-thickening behavior at high shear rates, followed by a maximum in the viscosity and a resumption of shear thinning. (Note that this latter effect is not noticeable in Fig. 3, as it was drawn on a large scale to depict trends in λ. However, Fig. 1 was actually generated by using $\lambda = 3$ as a parameter, and it is thus evident that this shear-thinning region at high shear rates is well-described by the model.) As λ continues to increase, above a value of about 100, the shear-thickening behavior is damped out and replaced again by shear thinning and then saturation, as was the case for $\lambda = 2$. This figure thus demonstrates that the shear-thickening behavior of the solutions only occurs when the relaxation times of the two modes are within two orders of magnitude of each other.

In Figure 4, we plot the dimensionless viscosity versus dimensionless shear rate for $\lambda = 3$, $\theta = 0.1$, and various values of n. This figure shows that there is also a concentration window within which the shear thickening appears. At values of n of 0.05 and 0.075, we observe the pattern of Figure 1: shear thinning, followed by shear thickening, and then shear thinning again. However, at the highest concentration, only shear thinning is evident. Also, although not shown on the graph because of scale, at lower concentrations, only shear thinning is evident as in the $n = 0.10$ case shown. Interestingly, this general behavior was observed in the experiments of Kishbaugh and McHugh,[1,2] who reported that shear thickening occurred within a certain concentration window for a particular solution, and above or below that window only shear thinning was observed. Evidently then, the appearance of a shear-thickening region of the flow curve is only possible under very special circumstances. These circumstances will become clear later.

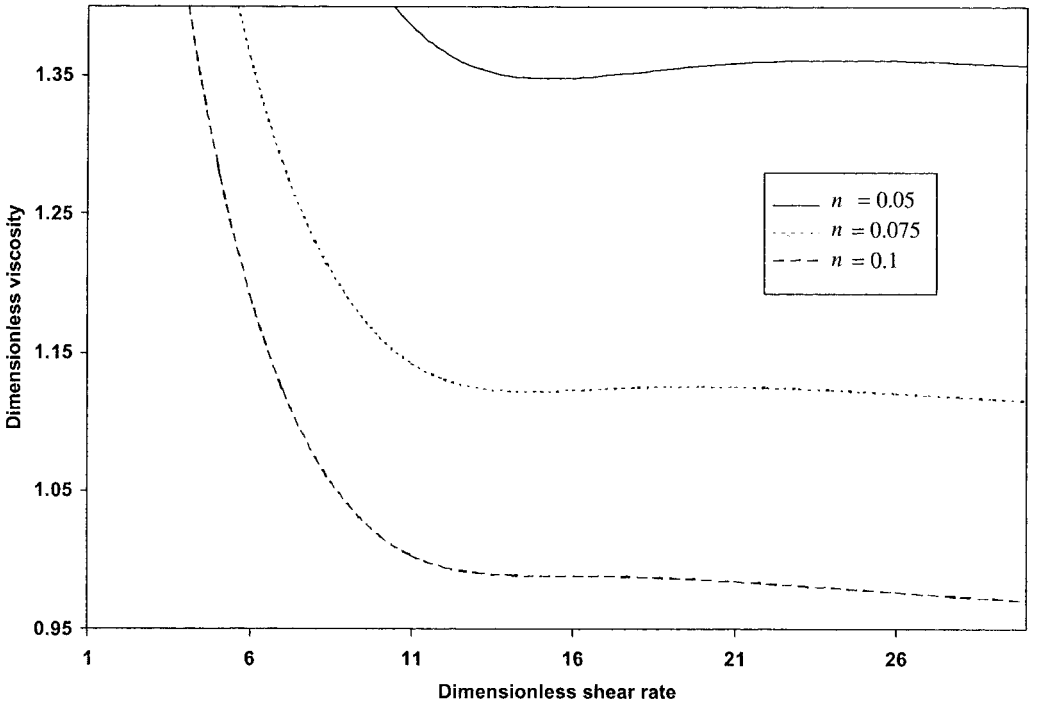

Figure 4 Dimensionless flow curves for $\lambda = 3$, $\theta = 0.1$, and various values of n.

Figure 5 depicts the dimensionless viscosity versus dimensionless shear rate for $\lambda = 3$, $n = 0.05$, and various values of θ. When $\theta = 0.0$, one recovers the behavior of the two uncoupled Maxwell modes model (i.e., a viscosity that is independent of shear rate). However, as shown in

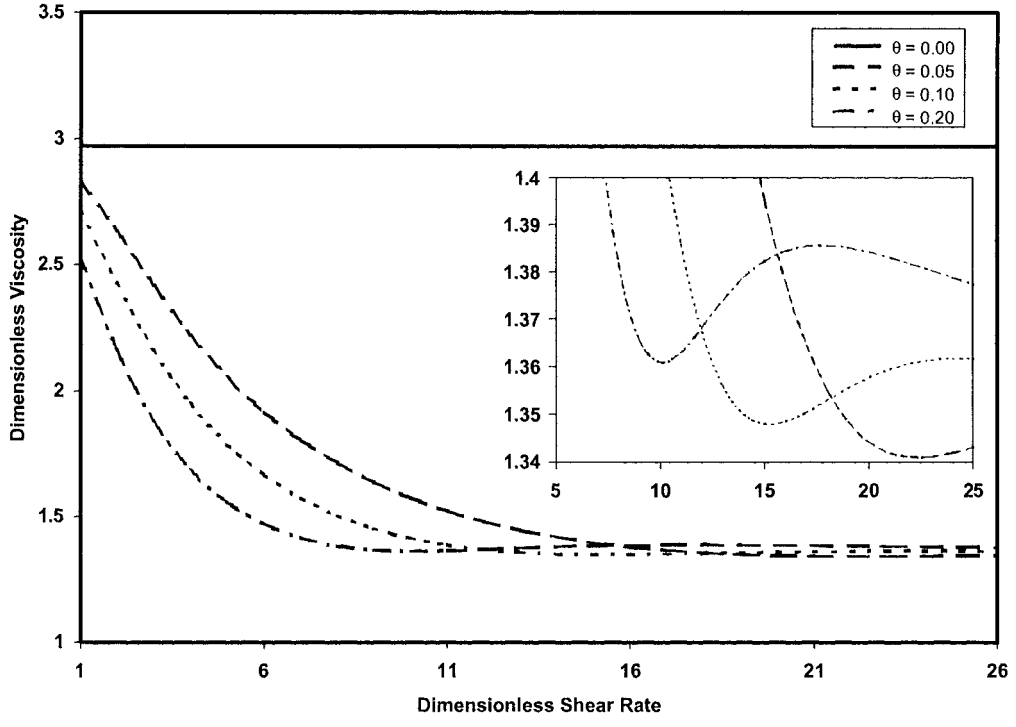

Figure 5 Dimensionless flow curves for $\lambda = 3$, $n = 0.05$, and various values of θ.

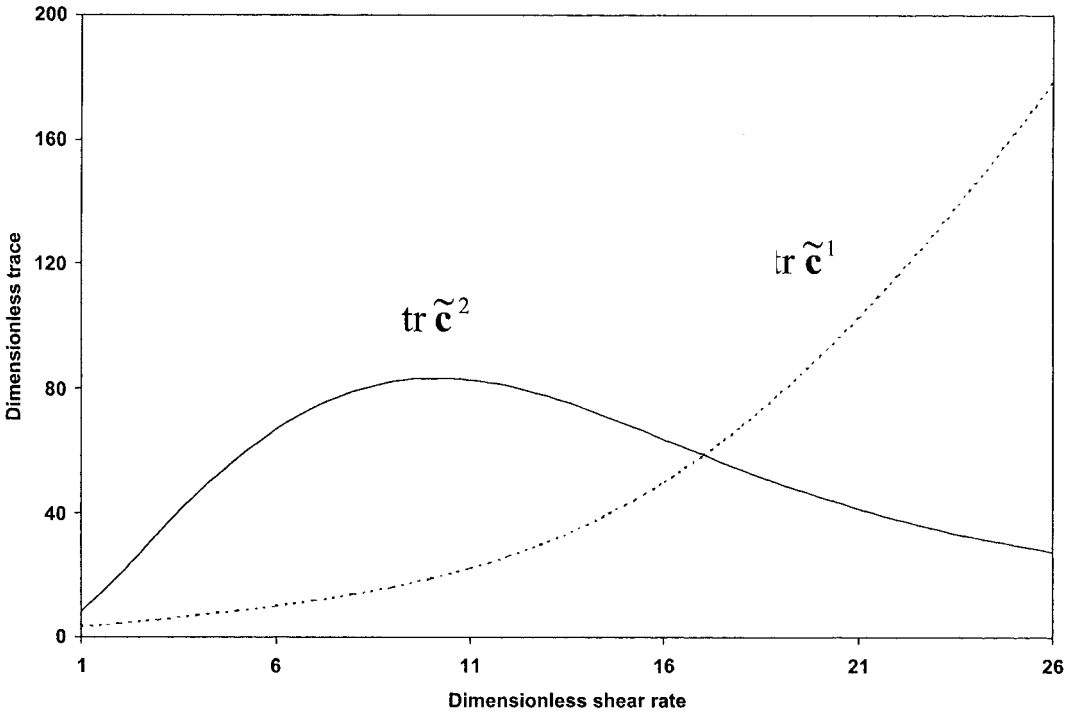

Figure 6 The traces of the dimensionless mode-conformation tensors versus dimensionless shear rate for $\lambda = 3$, $n = 0.05$, and $\theta = 0.1$.

the inset of Figure 5, for finite values of θ the flow curve develops a shear-thickening region at intermediate values of the shear rate. As θ continues to increase, the relative magnitude of shear thickening increases steadily, and the critical shear rate for the onset of this behavior moves to lower values of the dimensionless shear rate. The interaction parameter is thus shown to be critical for the observation of not only the shear-thickening region of the flow curve, but also for any shear-rate dependent rheological properties whatsoever.

Now let us examine the behavior of the two mode-conformation tensors for the case $n = 0.05$, $\lambda = 3$, and $\theta = 0.1$. This can give us important clues as to the development of the anomalous shear-thickening behavior. Figure 6 shows the behavior of the traces of the two mode-conformation tensors versus dimensionless shear rate. In essence, these are measures of the degree of orientation for the first mode, and the relative structure size (or aspect ratio) for the second mode: tr $\tilde{\mathbf{c}}^1 = \text{tr}\langle\mathbf{RR}\rangle/\text{tr}\langle\mathbf{RR}\rangle_0$ and $\text{tr}\tilde{\mathbf{c}}^2 = \text{tr}\langle\mathbf{aa}\rangle/\text{tr}\langle\mathbf{aa}\rangle_0$, where the angular brackets denote the averages defined in eqs. (1) and (2), and the subscript denotes that the averages are taken in the limit as $\dot{\gamma} \to 0$. The first mode, representing the individual molecular orientation and extension, increases without limit with increasing shear rate. This implies that the polymer molecules are further extended and oriented to a greater degree with increasing applied shear. The second mode, however, shows an unexpected behavior: the size of the structures increases only at low shear rates, reaches a maximum, and then decreases with increasing shear rate thereafter. By comparing the value of $\dot{\gamma}$ where this maximum occurs with the value at which the viscosity minimum occurs for the corresponding case in Figure 5, it is evident that the maximum occurs at a slightly lower value of the shear rate than the minimum.

If the model is to be believed then, this implies that the shear-thickening behavior observed in these solutions is caused not by the formation of supermolecular structures as in the Kishbaugh and McHugh hypothesis,[3] but instead by the degradation of that structure. The effect of this structure is, therefore, actually to reduce the effective shear stress in accordance with its intrinsic length scale: the larger the structure (i.e., the more elongated it is), the more it reduces the apparent shear stress. (We shall return to this line of reasoning later after comparing the model predictions with experimental data.)

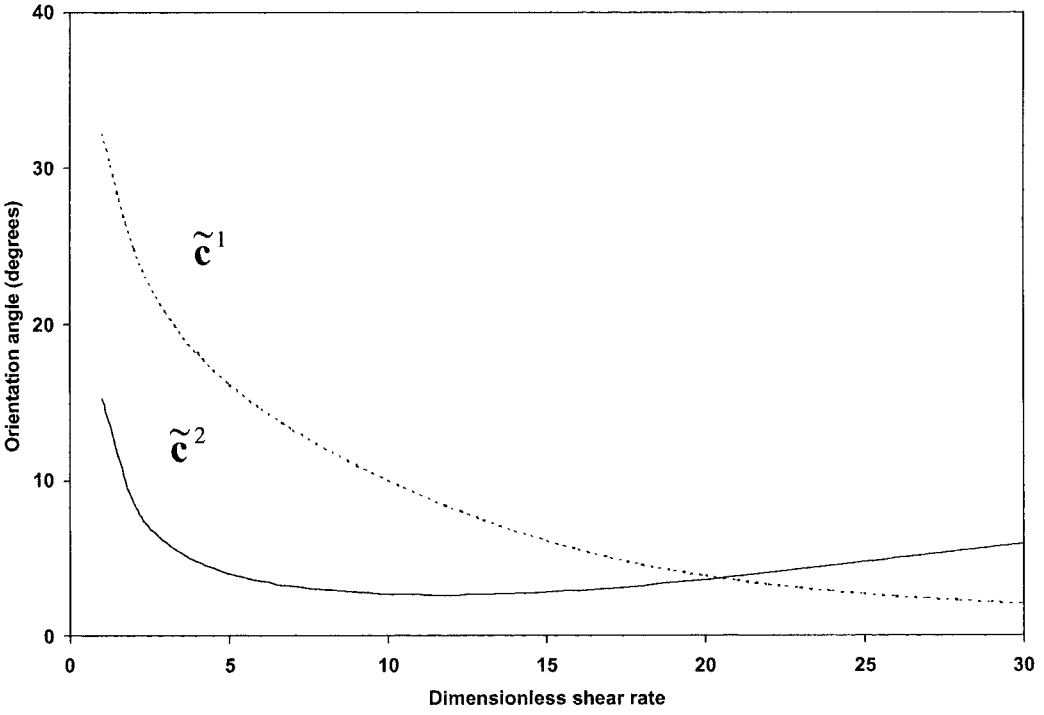

Figure 7 The orientation angles (degrees) of the two modes versus dimensionless shear rate.

In Figure 7, we plot the orientation angles of the two modes with respect to the direction of flow, in a counterclockwise progression. At low shear rates, both angles decrease rapidly from the value of 45° as $\dot{\gamma} \to 0$. For intermediate and high values of the shear rate, the first mode orients very close to the flow direction. On the other hand, the second mode orients along the flow direction to the greatest degree when the structure size is relatively large. As the aspect ratio of the structures decreases with increasing shear rate, the orientation angle increases marginally.

We can also use the model to predict the qualitative behavior of the dimensionless first and second normal-stress coefficients for these solutions, which were never measured experimentally. These are plotted versus dimensionless shear rate in Figure 8 for the case $n = 0.05$, $\lambda = 3$, and $\theta = 0.1$. Interestingly, the first normal-stress coefficient also exhibits a shear-thickening effect, whereas the second normal-stress coefficient does not. Hence, the structure size affects not only the shear stress, but also the normal stress tensor components as well. Note that the second normal-stress coefficient is a small negative fraction of the first normal-stress coefficient, in agreement with general trends in polymeric fluid dynamics.

COMPARISON OF THE TCMM MODEL WITH EXPERIMENTS

In this section, we continue our examination of this peculiar shear behavior by fitting the TCMM model to some of the experimental data of Vrahopoulou and McHugh[7] and Kishbaugh and McHugh.[2] To compare the model with experimental data, optimization of the five parameters is carried out after evaluating eqs. (3) and (4) over a range of shear rates.

Vrahopoulou and McHugh[7] present data for solutions composed of high molecular weight polyethylene in xylene and polypropylene in tetralin. The data are presented in terms of relative viscosity versus shear rate, and reduced viscosity versus shear rate. The relative viscosity, η_r, is the ratio of the solution viscosity, η, to the solvent viscosity, and is unitless. The reduced viscosity, η_{sp}/c, is expressed in units of dl/g, and is defined as

$$\frac{\eta_{sp}}{c} \equiv \frac{\eta_r - 1}{c} \tag{5}$$

where c is the solution concentration with units of g/dl. In this article, we only examine a sampling of

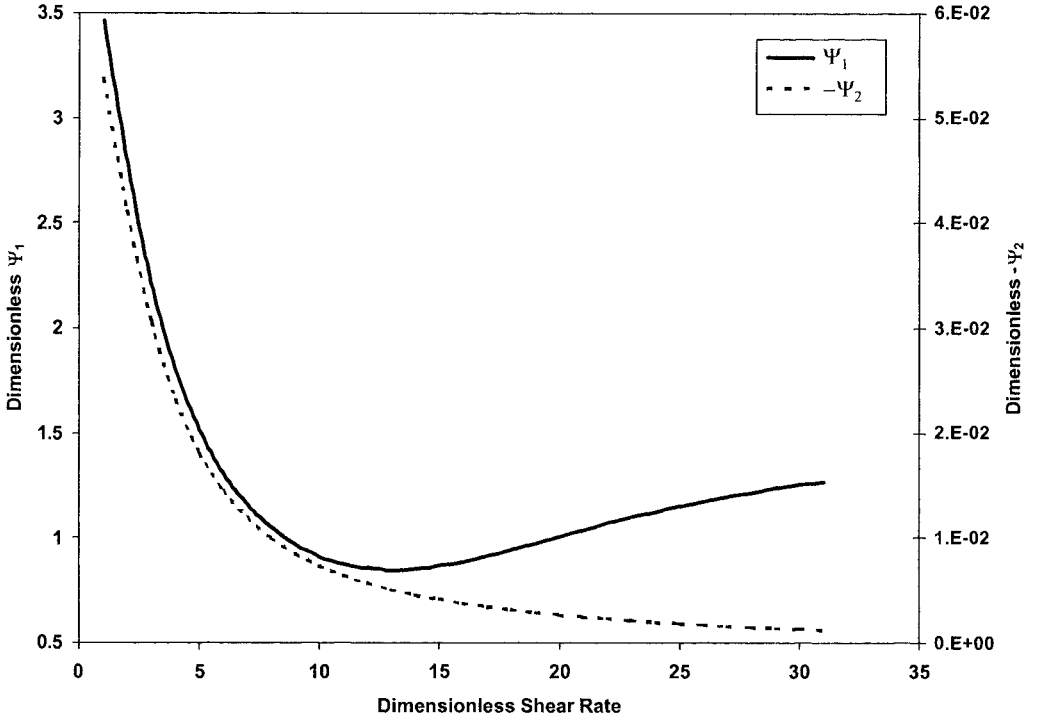

Figure 8 The dimensionless first and second normal-stress coefficients as functions of dimensionless shear rate for the case $n = 0.05$, $\lambda = 3$, and $\theta = 0.1$.

the data available in the literature. This will allow us to focus on the physics associated with the shear thickening without getting mired down in extensive data fitting. Future work will address a full parameterization of all available experimental data, allowing us to achieve a more thorough understanding of the variation of the mode parameters with concentration, temperature, molecular weight, and atomistic polymer structure.

Before comparing the model calculations with the experimental data, we must point out that the η_{sp}/c versus $\dot{\gamma}$ curves in ref. 7 were generated by taking c with units of (wt %) instead of g/dl. In consequence, all of the reduced viscosity curves in ref. 7 underestimate the actual values of η_{sp}/c. Herein, we use the corrected values for this quantity.

In Figure 9, we show the optimized fit of the model for the corrected polypropylene in tetralin data of Vrahopoulou and McHugh.[7] Table I lists the optimized parameter values for the three temperatures examined at a concentration of 0.01 wt %. (Note that we only examine the shear rate regions encompassing the initial shear-thinning and shear-thickening regions here because this is where all of the interesting physics takes place.) As evident from the figure, the model overpredicts the viscosity at low values of the shear rate and underpredicts it at high values. Nevertheless, the agreement is quite satisfactory with such a simple model. Most likely, we could improve the fit by incorporating more complicated features, such as shear-rate dependent relaxation times or variable mode concentrations, into the model, but these would only obscure the essential information that we are trying to investigate. Therefore, we are, at present, satisfied with our model fits to the experimental data.

We find that the model faithfully represents the general features of the experimental data. The viscosity decreases with increasing temperature for any particular value of the shear rate, and the minima of the viscosity curves occur at increasing $\dot{\gamma}$ as the temperature increases.

As one would expect, the mode relaxation times decrease with increasing temperature, as do the mode concentrations. One can easily rationalize why the concentration of the second mode would show this behavior: as the temperature increases, the individual molecules acquire a greater thermal kinetic energy, and the supermolecular structures are harder to form. The concentration of the first mode, representing the individual polymer chains, decreases with increasing temperature,

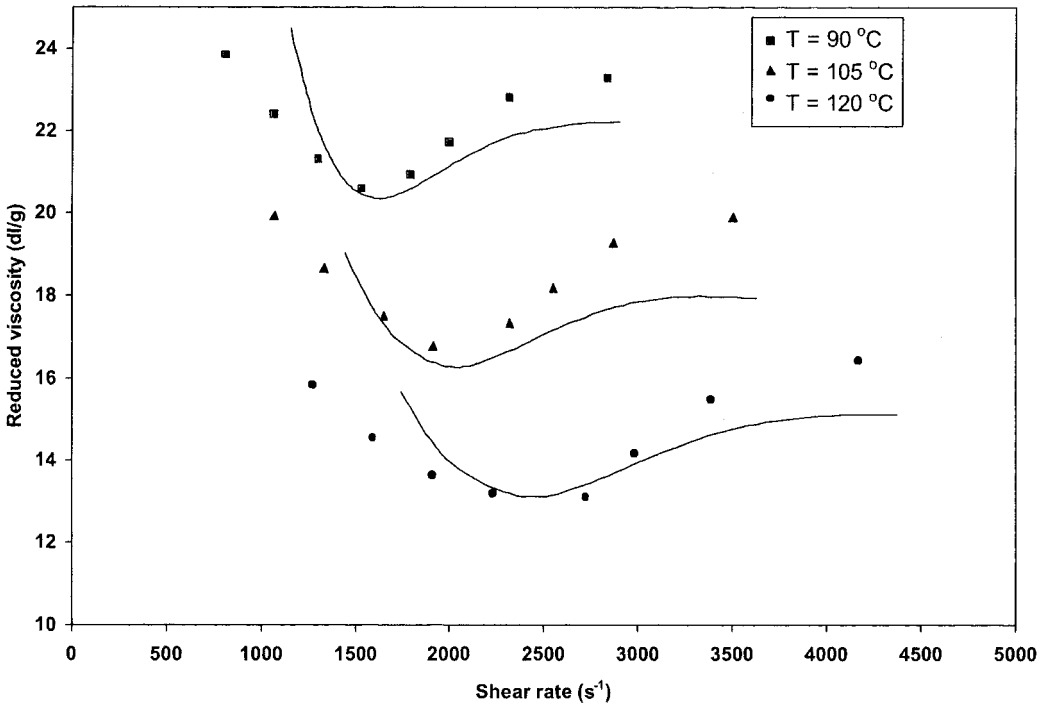

Figure 9 Model data fits for polypropylene in tetralin at the temperatures indicated and at a concentration of 0.01 wt % for the parameter values listed in Table I.

because the concentration in the experiments was expressed in weight percentage. Therefore, it varied with temperature because the density of the solvent varied with temperature. By using the value for the weight-average molecular weight, 3×10^6 g/mol, for the polypropylene used in ref. 7, we calculate quiescent concentrations of the first mode as 0.0306 mol/m^3 at 90°C, 0.0302 mol/m^3 at 105°C, and 0.0298 mol/m^3 at 120°C. The optimized concentrations for this mode are still two orders of magnitude below these values. If we were fitting data in the zero shear-rate limit where no (or very small) associations were forming, then we might have obtained higher values. At these high shear rates, however, the model optimization chose the best values for the parameters to fit the data over the entire shear-rate range under investigation.

The parameter θ was practically independent of temperature. This suggests that the degree of coupling between the two modes is not affected by the size of the structures formed under application of shear. (Note, though, that having a nonzero value of θ is absolutely required to obtain not only shear thickening, but any shear-rate dependent rheological properties whatsoever.)

With these curves thus parameterized, we can make predictions for the first and second normal-stress coefficients, which were unobtainable in these experiments. These are plotted in Figure 10. Figure 10(a) depicts the behavior of the first normal-stress coefficient plotted versus shear rate. This characteristic function decreases with increasing temperature and shows both shear-thinning and shear-thickening behavior in the same shear rate regimes as the shear viscosity

Table I Parameter Values for 0.01 wt % Polypropylene in Tetralin

T (°C)	λ_1 (s)	λ_2 (s)	n_1 (mol/m^3)	n_2 (mol/m^3)	θ
90	0.005	0.015	1.30×10^{-4}	5.62×10^{-6}	0.12
105	0.004	0.012	1.18×10^{-4}	5.20×10^{-6}	0.12
120	0.0033	0.010	1.17×10^{-4}	5.00×10^{-6}	0.12

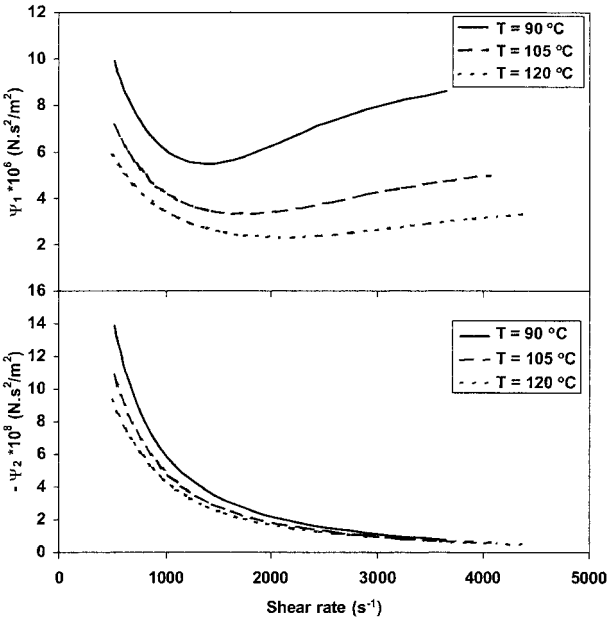

Figure 10 Model predictions for the first and second normal-stress coefficients versus shear rate for polypropylene in tetralin at the temperatures indicated.

curves. The magnitude of this quantity is rather small, leaving little hope at the present time of obtaining any reliable measurements of its value. The second normal-stress coefficient predicted by the model is displayed in Figure 10(b). It displays only shear-thinning behavior, is negative in value, and its relative magnitude is two orders less than that of Ψ_1.

More extensive data, containing both viscosity and optical measurements, can be found in the article of Kishbaugh and McHugh[2] for solutions of high molecular weight polystyrene in decalin. Here, we examine only one of the samples tested in refs. 1 and 2, and only two different concentrations—one in this section, and one in the penultimate one. Again, a full parameterization of all the available experimental data would only obscure the important physical information in a barrage of parameter values, so we shall consider the parameterization of these additional data sets in future work.

The sample we shall consider has a weight-average molecular weight of 6.8×10^6 g/mol, and in this section we consider the solution of concentration 0.25 g/dl at a temperature of 25°C. At this concentration, one would expect that the fluid contained roughly 0.00368 mol/m^3 of polymer.

Figure 11 depicts the TCMM model fit to the shear viscosity, linear dichroism, and the dichroic orientation angle for this solution with the parameter values given in the figure caption and specified in Table II. To obtain this figure, the five parameters were fit to the shear viscosity curve only, and the remaining curves generated by using those values, as given in Table II, in the manner explained below. Once again, note that the model overpredicts the shear viscosity at low shear rates and underpredicts it at high ones. Most interesting, however, is the optical behavior. Note that the dichroism displays a maximum at about the same shear rate as the minimum in the viscosity curve and decreases in magnitude thereafter. At very high shear rates, it crosses the shear-rate axis and becomes negative. Also, the orientation angle decreases at low shear rates, levels off at intermediate ones, and then increases gradually at high shear rates until an abrupt drop in value occurs at a very high shear rate. The model provides an accurate qualitative description of the solution behavior, and a reasonable quantitative fit as well, all things considered.

The dichroism and its orientation angle were computed by using the same five parameter values that were fitted to the viscosity curve. The dichroism was assumed to arise from two sources: Rayleigh scattering from the structures and the innate dichroism of the individual molecules. Thus, both modes contribute to the dichroic signal, $\Delta n''$, the expression for which is divided into two contributions, $\Delta n'' = \Delta n''_1 + \Delta n''_2$, where[3]

$$\Delta n''_1 = \frac{4\pi}{5} k^3 \frac{cN_A m_s}{M} (\alpha_1^2 - \alpha_2^2)_1 [\mathrm{tr}\, \tilde{\mathbf{c}}^1 - 3] \quad (6)$$

and

$$\Delta n''_2 = \frac{8\pi}{15} m_p n_2 N_A k^3 (\alpha_1^2 - \alpha_2^2)_2 \frac{b}{(1 + 36/\sigma^2)} \quad (7)$$

The first expression, eq. (6), is the innate dichroism of the deformed polymer chains.[3] The quantities appearing therein are the wavenumber, $k \equiv 2\pi/(6.328 \times 10^{-7}\ \mathrm{m})$; the polymer concentration, c; the molecular weight, M; the refractive index of the solvent, $m_s = 1.474$; and the polarizability difference, $(\alpha_1^2 - \alpha_2^2)_1 = -1.25 \times 10^{-42}$ cm^6/molecule. Kishbaugh and McHugh[1,3] computed the value of this last quantity by using the method of Gurnee.[19] However, we have found that their rationalization is not particularly satisfying because the method is not exact and an order of magnitude error in the value of this

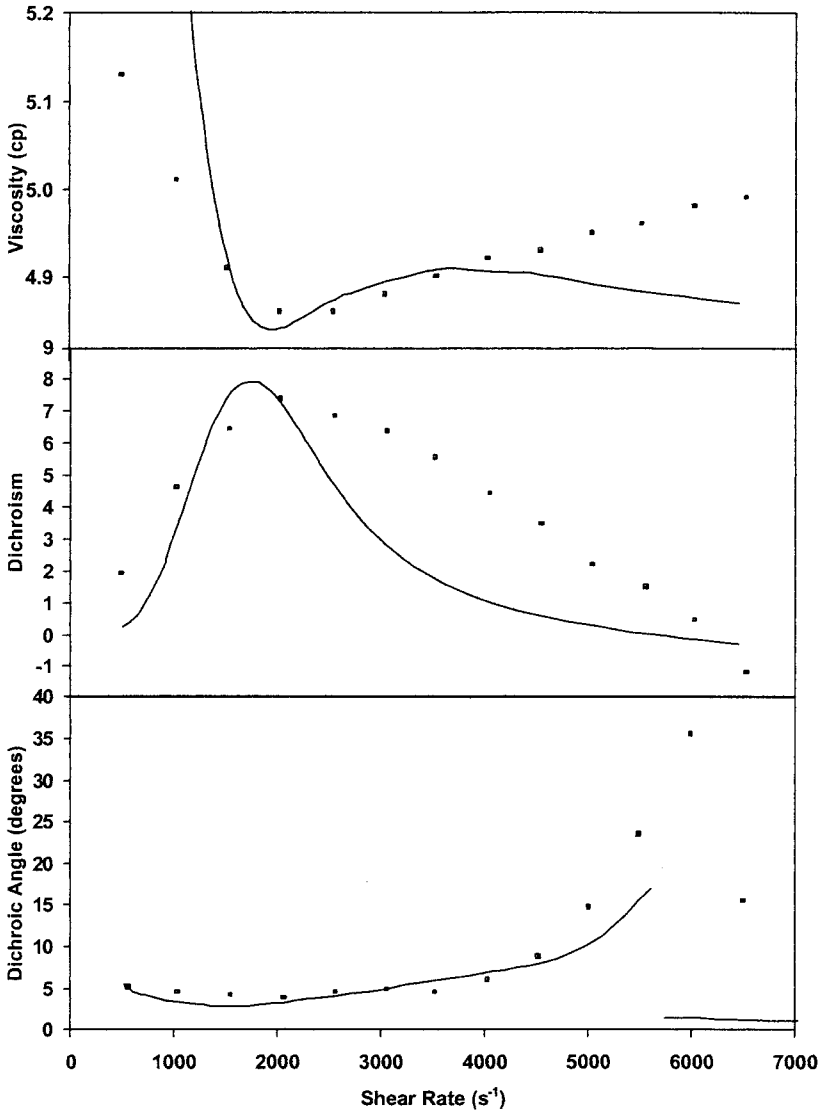

Figure 11 The TCMM fit of the experimental viscosity, linear dichroism, and dichroic orientation angle for the 0.25 g/dl solution of polystyrene in decalin. Parameter values used to obtain the fit are $\lambda_1 = 0.004$ s, $\lambda_2 = 0.012$ s, $n_1 = 9.3 \times 10^{-4}$ g/dl, $n_2 = 5.0 \times 10^{-5}$ g/dl, and $\theta = 0.12$.

quantity produces unrealistic results. The two quantities, α_1 and α_2, are so small that computing their squares is fraught with large errors.[1,3] The value of this parameter is then assumed to be independent of concentration and used in the calculations for the 0.30 dl/g solution below. It turns out that $\Delta n''_1$ is only important at very low and very high shear rates.

The second term in eq. (6) is the dichroism arising from the supermolecular structures ac-

Table II Parameter Values for Polystyrene in Decalin at 25°C

c (g/dl)	λ_1 (s)	λ_2 (s)	n_1 (mol/m^3)	n_2 (mol/m^3)	θ	$\langle \mathbf{aa} \rangle_0$ (m^2)
0.25	0.004000	0.012	9.3×10^{-4}	5.0×10^{-5}	0.12	3.06×10^{-16}
0.30	0.004333	0.013	1.0×10^{-3}	1.0×10^{-6}	0.10	4.20×10^{-16}

cording to the Rayleigh scattering theory.[3] The quantities appearing in this expression are the refractive index of the polymer, $m_p = 1.59$, and several other functions. The first is an anisotropy function that depends on the sphericity or shape of the structure, p:

$$b = \frac{p^2 - 1}{p^2 + 1} \tag{8}$$

with p taken as

$$p = \left(1 + \frac{3}{2}\left[\text{tr}\ \tilde{\mathbf{c}}^2 - 3\right]\right)^{3/4} \tag{9}$$

The quantity σ is a dimensionless measure of the shear rate relative to the size and shape of the assumed structures. It is given by[3]

$$\sigma = \frac{\eta_S V_p \nu(p)}{k_B T}\,\dot{\gamma} \tag{10}$$

where V_P is the volume of the structure

$$V_P = \frac{4\pi}{3p^2}\,a^3 = \frac{4\pi}{3p^2}\left(\left[\text{tr}\ \tilde{\mathbf{c}}^2 - 3\right]\langle\mathbf{aa}\rangle_0\right)^{3/2} \tag{11}$$

and

$$\frac{1}{\nu(p)} = \frac{p^2}{p^4 + 1}\left(-1 + \frac{2p^2 - 1}{2p\sqrt{p^2 - 1}}\ln\left[\frac{p + \sqrt{p^2 - 1}}{p - \sqrt{p^2 - 1}}\right]\right) \tag{12}$$

Note that $\langle\mathbf{aa}\rangle_0$ is a parameter that is fit to the dichroism curve by matching the maximum value of $\Delta n''$ at the appropriate shear rate. After fitting, a can be used to determine the effective structure size at any shear rate by taking the square root of the primary eigenvalue of $\tilde{\mathbf{c}}^2$ multiplied by the factor $\langle\mathbf{aa}\rangle_0$: $a = \sqrt{(\lambda_p - 1)\langle\mathbf{aa}\rangle_0}$.

The last quantity appearing in eq. (7) is the polarizability difference of the structures, $(\alpha_1^2 - \alpha_2^2)_2$. It is given by

$$\frac{16\pi^2}{V_P^2}\,(\alpha_1^2 - \alpha_2^2)_2 = \left(\frac{1}{L_1 + 1/(m_s^2 - 1)}\right)^2 - \left(\frac{1}{L_2 + 1/(m_s^2 - 1)}\right)^2 \tag{13}$$

where

$$L_1 = \frac{1 - e^2}{e^2}\left(-1 + \frac{1}{2e}\ln\left[\frac{1 + e}{1 - e}\right]\right) \tag{14}$$

$$L_2 = \frac{1 - L_1}{2} \tag{15}$$

$$e^2 = \left(1 - \frac{1}{p^2}\right) \tag{16}$$

The orientation angle of the dichroism is calculated by determining which mode is dominating the dichroism. During the shear-thickening region of the flow curve, the structures dominate the dichroism, and the orientation angle of the dichroism is that of the second mode. At very high shear rates, after the structures were reduced to isotropic spheroids, the individual chains dominate the dichroism and the orientation angle switches to that of the first mode.

The effective structure size a is plotted versus shear rate in Figure 12. This curve was calculated by fitting the parameter $\langle\mathbf{aa}\rangle_0 = 3.06 \times 10^{-16}\ \text{m}^2$ to the dichroic maximum value at the critical shear rate. This demonstrates that the size of the structures is increasing with shear rate at low shear rates, until the size becomes so large and extended that the shear forces tend to reduce their aspect ratio. This causes the maximum in the linear dichroism curve. These structures are quite extended and range in size from about a hundredth to a tenth of a micron over the shear-rate range examined. After the structure is completely spheroidal at very high shear rates, the innate dichroism of the individual molecules is all that remains, and this is inherently negative. This causes the crossover to negative values of the dichroism at very high shear rates. Furthermore, at low shear rates, the orientation of the structures decreases toward a saturation value very close to the flow direction. As the structures begin to be reduced in size at higher shear rates, the orientation angle increases with increasing shear rate, until the structures are spherical and the orientation angle drops precipitously to that of the individual molecules.

The TCMM model descriptions of the linear birefringence, $\Delta n'$, and its orientation angle are depicted in Figure 13. The birefringence is calculated according to

$$\Delta n' = 2\pi\,\frac{n_1 N_A}{50}\,m_s\left(\left[\text{tr}\ \tilde{\mathbf{c}}^1 - 3\right]\Theta_i + \left[\text{tr}\ \tilde{\mathbf{c}}^1 - 3\right]\Theta_{fs} + 4\pi e_1\Theta_f\right) \tag{17}$$

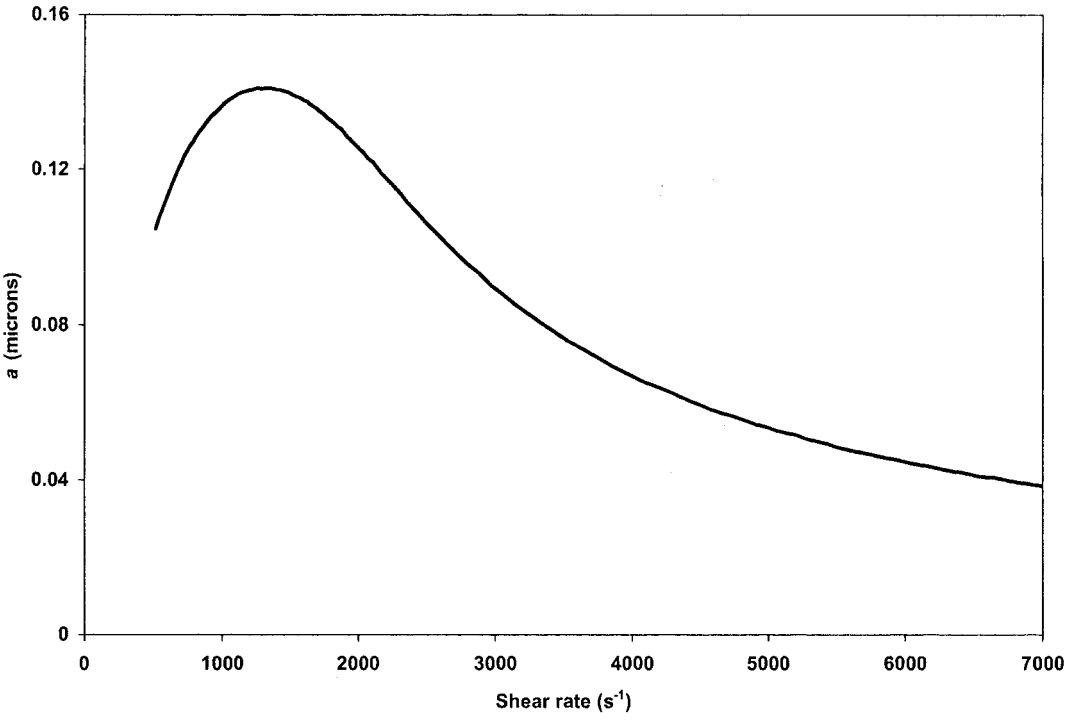

Figure 12 Model prediction for the average size of structures versus shear rate for the 0.25 g/dl polystyrene in decalin solution under consideration.

where it is assumed that only the first mode has any appreciable effect on the birefringence. (This assumption was tested by Kishbaugh and McHugh,[3] and also by the present authors, by calculating the birefringence arising from the second mode in Rayleigh scattering theory. We will not describe this calculation here because the result did not affect the value of the total birefringence.) A factor of 50 occurs in the denominator of eq. (17) to bring the prediction of (17) in line with the experimental data. In other words, it allows the result of calculation with eq. (17) to be on the same order of magnitude with the experimental birefringence. It should thus be viewed as an additional fitting parameter; however, once its value is set for any one of the polystyrene/decalin solutions at a given concentration, it should not change as concentration, temperature, or polymer molecular weight is varied.

In the above expression, three types of phenomena contribute to $\Delta n'$. The first of these is the intrinsic optical anisotropy of the polymer chains. This effect is represented through Θ_i, which is given by[20]

$$\Theta_i = \frac{3}{5}(\alpha_1 - \alpha_2)_1 \tag{18}$$

The polarizability difference, $(\alpha_1 - \alpha_2)_1 = -5.49 \times 10^{-24}$ cm^3/molecule, is assumed to have the value estimated by Kishbaugh and McHugh,[3] according to the method of Gurnee.[19] [As alluded to above, there may be up to two orders of magnitude of uncertainty in this quantity, and this explains the magnitude corrector (50) in Eq. (17).] The intrinsic optical anisotropy of polystyrene is thus a negative quantity.

The second contributor to the overall birefringence is the macroform anisotropy,[21] which is caused by the difference between the refractive indices of the polymer and solvent. In eq. (17),

$$\Theta_f = \left(\frac{m_s^2 + 2}{3}\right)^2 \left(\frac{m_p^2 - m_s^2}{4\pi m_s \rho N_A}\right)^2 \frac{M^2}{\nu} \tag{19}$$

$$e_1^2 = \left(1 - \frac{1}{p_1^2}\right) \tag{20}$$

where $\rho = 1.065$ g/ml, and $M^2/\nu = 1.543 \times 10^{28}$ g/mol for polystyrene at the specified value of M (6.8×10^6 g/mol). Note, however, that p_1 appearing in eq. (20) is now a function of the trace of the first mode-conformation tensor, instead of the second, $p_1 = (1 + 3/2\ [\mathrm{tr}\ \tilde{\mathbf{c}}^1 - 3])^{3/4}$.

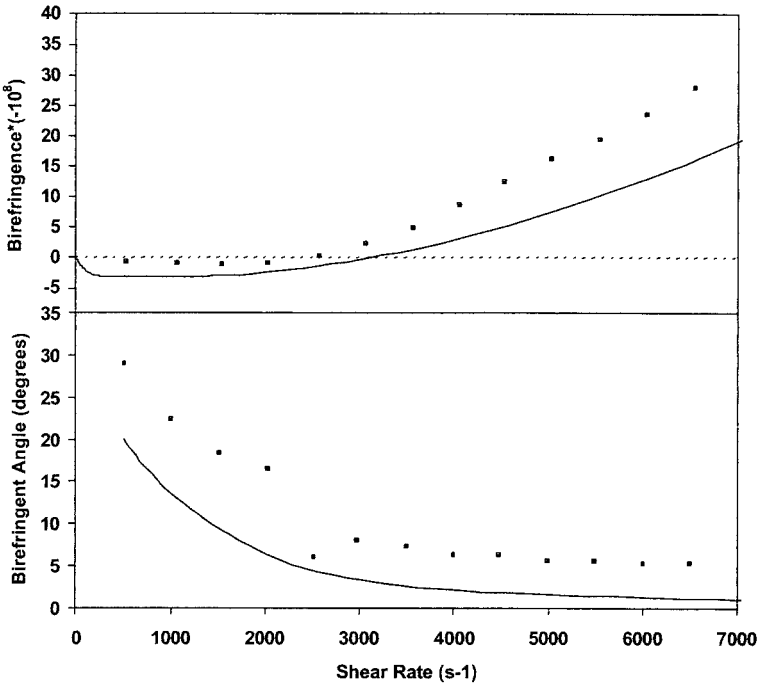

Figure 13 The birefringence and its orientation angle versus shear rate for the 0.25 g/dl solution of polystyrene in decalin.

The third contribution to the birefringence is the microform anisotropy,[22] which increases with the extension of the polymer chain. It is taken as

$$\Theta_{fs} = \frac{3}{5}\left(\frac{m_s^2 + 2}{3}\right)^2 \left(\frac{m_p^2 - m_s^2}{4\pi m_s}\right)^2 \frac{4\pi M_0 \zeta e_s}{\rho N_A} \quad (21)$$

where $\zeta = 5.4$ is the number of monomeric units per statistical chain segment, $M_0 = 104$ g/mol is the monomer molecular weight, and $e_s = 0.1$ is the optical shape factor for the segment.[3] Note that in the above expressions, no fitting parameters appear beyond the five that were used to fit the TCMM model to the shear viscosity versus shear rate curve and the magnitude corrector in eq. (17).

The effect of the macroform and microform anisotropies is always positive and is dominant at low shear rates where the polymer chains are not extended or oriented to any large degree. However, at intermediate shear rates, the intrinsic birefringence of the polymer chains begins to dominate the response as the chains become more and more extended and oriented along the flow direction. This causes the sign change seen in Figure 13. Considering that no additional parameters were used for this calculation, other than the magnitude corrector, the agreement between the model prediction and the experimental data are quite reasonable. If we had used the corrector as a true fitting parameter, we could have gotten much better agreement; however, there seemed to be no point in doing so.

The orientation angle of the birefringence is also plotted in Figure 13. This angle was calculated directly from the eigenvectors of $\tilde{\mathbf{c}}^1$. The theoretical prediction follows very closely the behavior of the experimental data: it decreases rapidly from its zero shear rate limit of 45° with increasing shear rate and saturates very near to the direction of flow.

Predictions for the first and second normal-stress coefficients for the 0.25 g/dl solution are ventured in Figure 14. The same qualitative behavior is seen here as for the polypropylene solutions examined earlier.

A DISCUSSION OF THE DIFFERENCES BETWEEN THE MODEL BEHAVIOR AND THE KISHBAUGH AND MCHUGH HYPOTHESIS

Kishbaugh and McHugh[3] hypothesized that the shear thickening is manifested in the viscosity

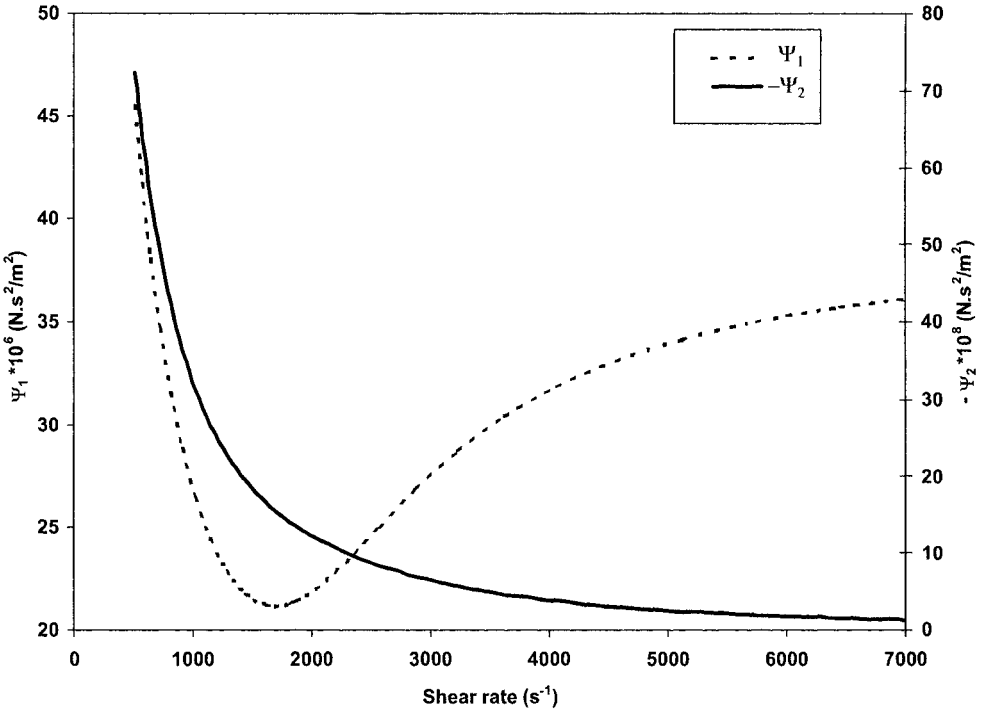

Figure 14 The first and second normal-stress coefficients for the 0.25 g/dl solution of polystyrene in decalin.

curve because of the growth of optically isotropic particles at high shear rates. Before the critical shear rate where the shear-thickening behavior manifests, the solutions begin to develop micron-size particles composed of amorphous polymer chains that orient along the flow direction. These particles grow in size with increasing shear rate, and, according to the ADA light scattering theory, this causes the maximum in the linear dichroism curve.[3] However, most polymer chains remain in solution, not in the particles, and it is the extension and orientation of these that cause the monotonic increase in the linear birefringence with increasing shear rate.

Kishbaugh and McHugh were led to this hypothesis by two notions, one experimental and one theoretical. The experimental one is that more concentrated solutions of these polymers than those discussed above can experience a flow-induced phase separation at large values of the shear rate.[23–27] Hence, it seemed reasonable that the precursor stage to this phenomenon was causing the shear thickening. Once the phase separation occurred, the separated phase was optically isotropic and plainly visible to the naked eye.[25–27] Thus, it seemed reasonable to rationalize that the shear thickening arose from the growth of optically isotropic particles and that the continued growth of these particles with increasing shear rate would eventually lead to phase separation at higher concentrations. Rather than pursue this idea here, however, we postpone this discussion until the next section of the article.

The theoretical notion leading to the Kishbaugh and McHugh hypothesis derived from the ADA scattering theory of Meeten,[28–31] and it is the subject of the present section. Under the auspices of this theory, the linear dichroism of the scattering centers is essentially a function of three variables: the concentration of particles, n_2; the shape of the particles, p; and the size of the particles, a. The theory is valid for particle sizes that are large relative to the wavelength of the incident light. In the present case, the wavelength is $\lambda_i = 6.328 \times 10^{-7}$ m, so the theory is valid when $2\pi a/\lambda_i$ is large, which implies that the scattering particles must be micron-size or larger for the theory to be valid.

The results of the ADA show that for fixed n_2 and p, the dichroism varies sinusoidally with increasing particle size a. Consequently, Kishbaugh and McHugh[3] fit the ADA during the first half-period of its sinusoidal cycle in a to their linear dichroism data for the 0.25 g/dl polystyrene

solution by using n_2, p, and a as fitting parameters. For fixed values of the first two parameters, they then could plot $\Delta n''$ versus particle size a. They found that the dichroism data versus shear rate could be fit well if a varied between 1.5 and 4 μm, with $n_2 = 9.46 \times 10^{-14}$ mol/m^3 and $p = 1.45$. Comparing this with the experimental data, they could then correlate increasing particle size with increasing shear rate.

Interestingly, the experimental data reveal that the maxima in the dichroic curves always correlate closely with the minima in the viscosity curves. However, there is nothing in the above hypothesis that explains why this must be the case: the particle size increases throughout the shear rate range under investigation. In this viewpoint, therefore, this correlation must be considered as coincidental.

In the TCMM model, one does not have as much freedom with the ADA, because two of the fitting parameters used above, n_2 and p, are determined by the model. The first is given by the original fit of the model to the viscosity data, and the second is determined by the second mode-conformation tensor [see eq. (9)]. Therefore, the only fitting parameter in the TCMM ADA calculation is the parameter $\langle \mathbf{aa} \rangle_0$. For micron-size particles, we found that the calculation produced dichroic behavior with many periods over the appropriate shear-rate range. This is so because p becomes larger, with increasing shear rate, than the constant value assumed in ref. 3, and because the value of n_2 that is required to fit the viscosity data is much larger than the value assumed in ref. 3 (see Table II). With such a large value for the concentration of structures, to get sensible results one must have much smaller structures, for which the ADA is no longer valid. Thus, when using the TCMM model, we were forced to use the Rayleigh scattering theory to explain the behavior of the linear dichroism. This theory is valid when the particle size is approximately $\lambda_i/20$, which is exactly the order of magnitude for a that fit the experimental dichroic data.

Because the particle size actually begins to decrease, and does not continue to increase, at the minima on the viscosity curves, the TCMM model provides a rational explanation as to why the viscosity minima and dichroic maxima always occur at approximately the same shear rates, whereas the ADA does not. Furthermore, the orientation angle in the ADA associated with the Kishbaugh and McHugh dichroism saturates along the flow direction,[3] whereas the experimental data clearly does not (see Fig. 11). Again, one is forced to the TCMM model to obtain the proper qualitative behavior for this quantity.

A DISCUSSION OF THE RELATIONSHIP BETWEEN SHEAR THICKENING AND PHASE SEPARATION IN POLYMER SOLUTIONS

As mentioned earlier, as one increases the concentration of the polymer in solution, a threshold will be crossed where no further shear thickening is observed: purely shear thinning is evident over the entire flow curve. If we increase the concentration of the solution under consideration to 0.30 g/dl, we see the experimental manifestation of this phenomenon in Figure 15.[1,2]

For these higher concentrations, where the purely shear-thinning behavior resumes, Kishbaugh and McHugh[3] argue that the structures do not form because they would be too large to be supported by the shear field. This is hard to accept because at even higher concentrations, a flow-induced phase separation can occur.[23–27] Obviously then, some associations are forming, which eventually phase separate from the bulk solution. Furthermore, if the structures cause shear thickening and none are forming, then why is the viscosity of the 0.30 g/dl solution higher than that of the 0.25 g/dl solution (compare Figs. 11 and 15) in the shear-rate region where the latter solution exhibits shear thickening? Let us examine what the TCMM model has to say about this phenomenon.

As evident in Figure 15, the TCMM model also fits the experimental viscosity data reasonably well for this purely shear-thinning solution with the parameter values listed in Table II. The dichroism saturates at high shear rates, as does the orientation angle. However, the interesting thing about the model predictions is that, instead of predicting a total lack of structures or very small ones, the model actually predicts that structures are formed. These structures are much larger, but less numerous, than in the 0.25 g/dl solution (see Fig. 16). Furthermore, these structures are not reduced in size by the increasing shear rate, as was the case for the 0.25 g/dl solution. Hence, no shear thickening is observed for the 0.30 g/dl solution.

The above analysis provides a rational explanation for flow-induced phase separation in polymer solutions. At high enough concentrations,

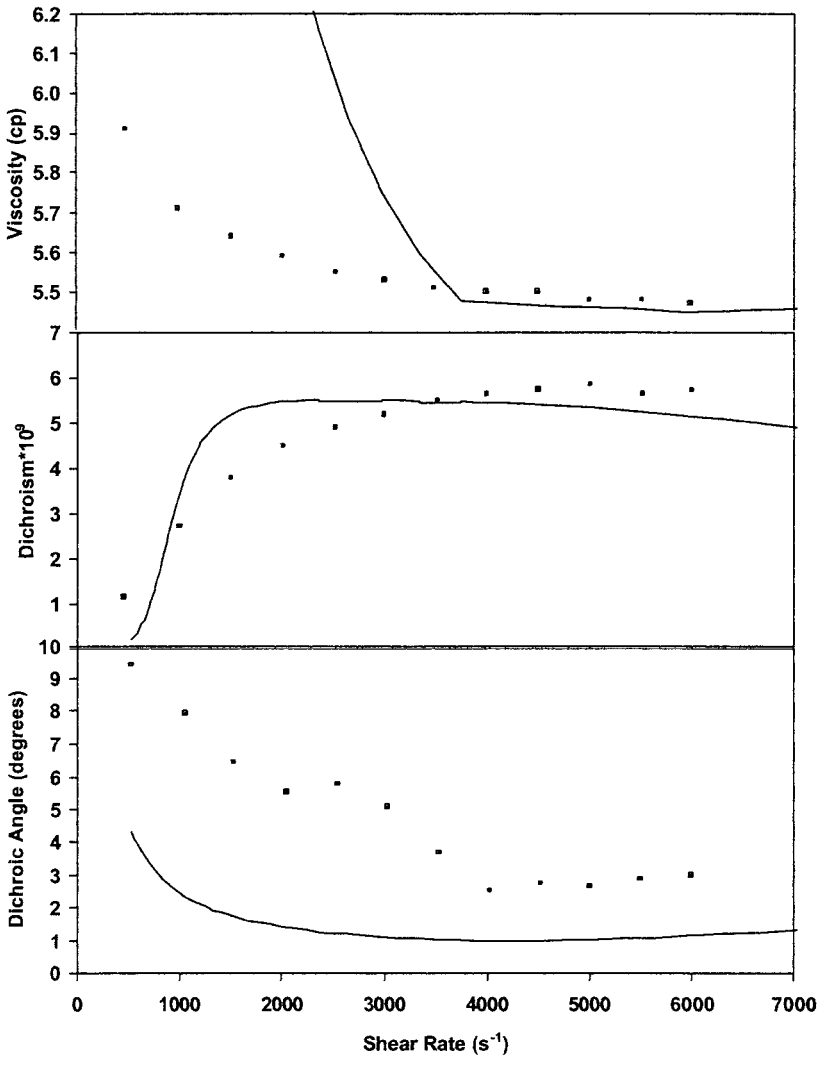

Figure 15 The TCMM fit of the experimental viscosity, linear dichroism, and dichroic orientation angle for the 0.30 g/dl solution of polystyrene in decalin. Parameter values used to obtain the fit are $\lambda_1 = 0.004333$ s, $\lambda_2 = 0.013$ s, $n_1 = 1.0 \times 10^{-3}$ g/dl, $n_2 = 1.0 \times 10^{-6}$ g/dl, and $\theta = 0.10$.

structures form under shear that become so large that the shear forces cannot affect them. Therefore, at some critical size and shear rate, phase separation is instigated. At lower concentrations, the structures never grow to a size appreciable enough to start phase separation because they are sheared down by the applied deformation.

For completeness, we also show the birefringence data and model fit for the 0.30 g/dl solution in Figure 17. As was the case for the 0.25 g/dl solution, the agreement is remarkably good considering that no additional parameters, other than the magnitude corrector, are used to fit the data beyond those needed to fit the shear viscosity. Predictions for the first and second normal-stress coefficients are given also in Figure 18. Note that there is no apparent shear thickening in the first normal-stress coefficient for this solution.

CONCLUSIONS

The TCMM model suggests a consistent, rational explanation for every facet and nuance of the rheological and optical behavior associated with shear thickening in dilute polymer solutions. Furthermore, it offers sensible predictions for rheological properties that cannot be measured exper-

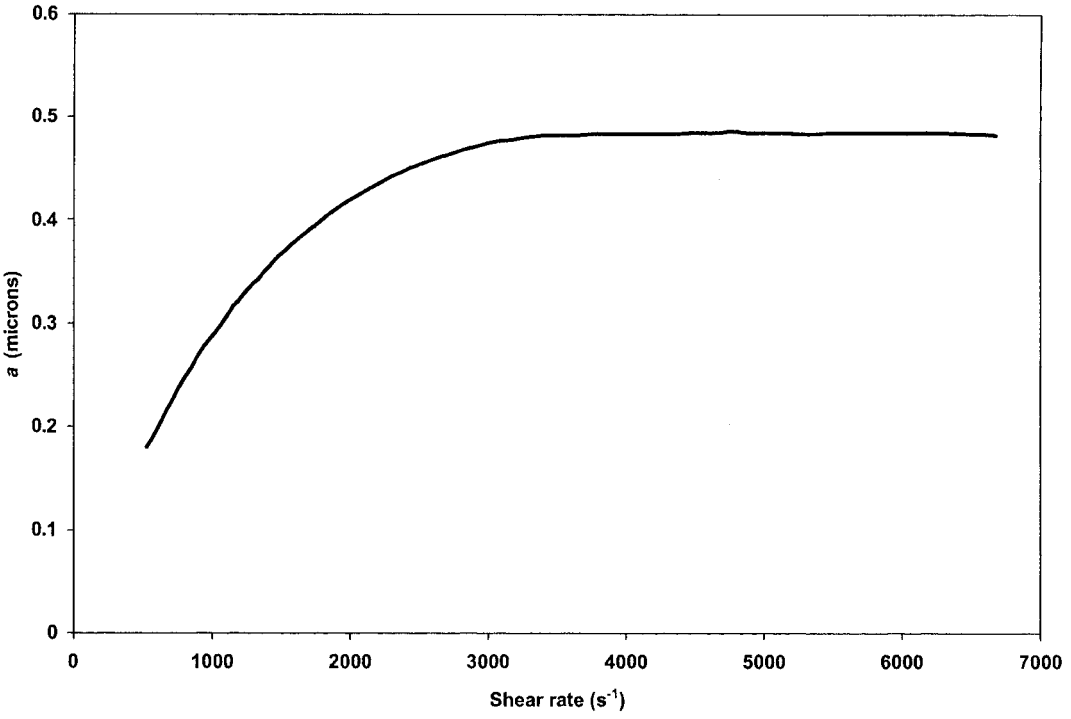

Figure 16 Structure size versus shear rate for the 0.30 g/dl polystyrene solution.

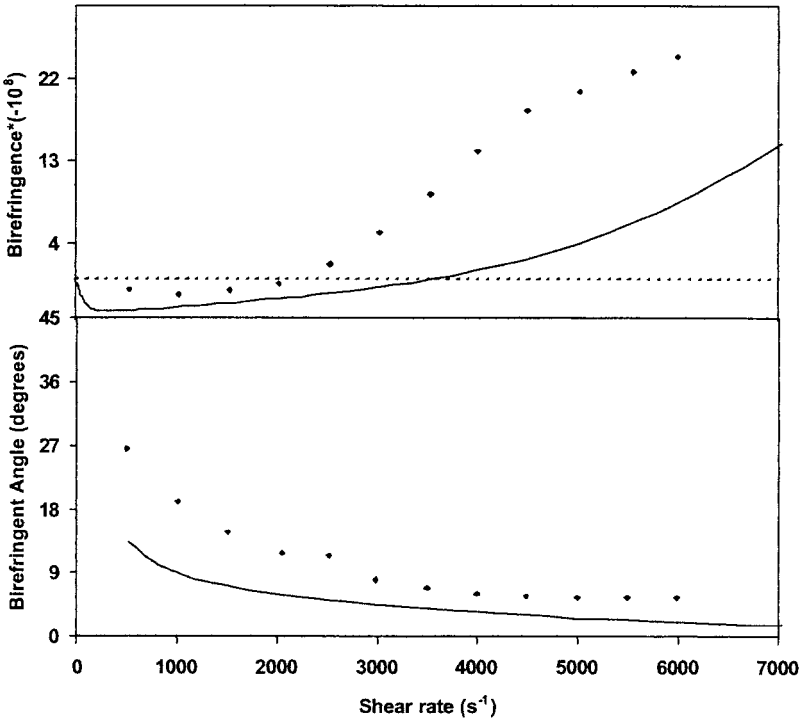

Figure 17 Linear birefringence and its orientation angle versus shear rate for the 0.30 g/dl polystyrene solution.

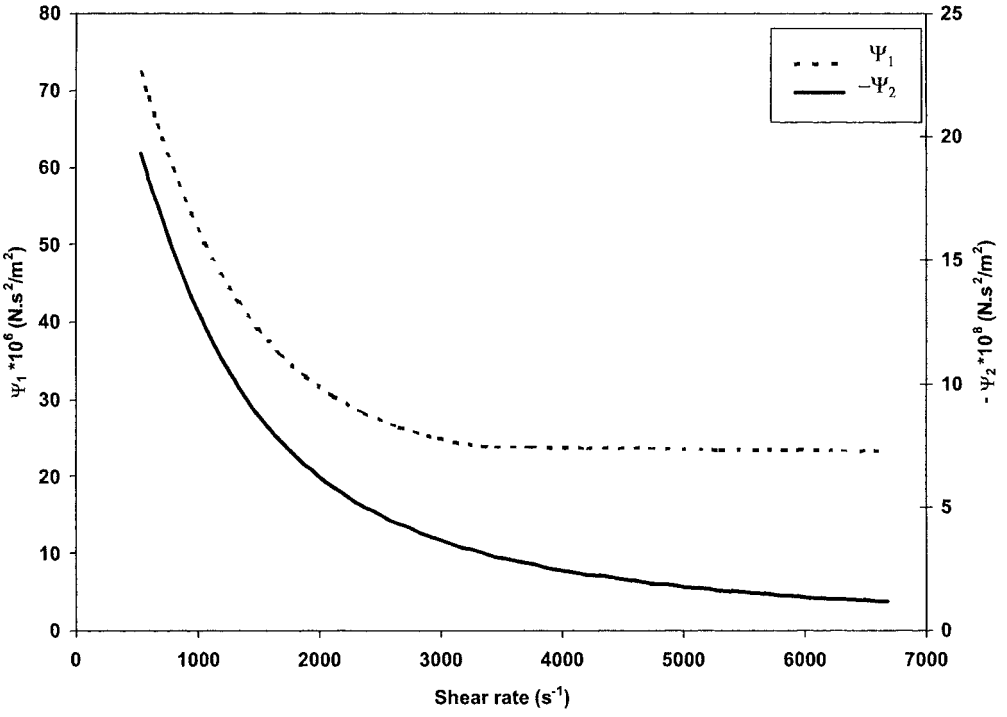

Figure 18 The first and second normal-stress coefficients versus shear rate for the 0.30 g/dl polystyrene solution.

imentally because of apparatus limitations. The main conclusions of this article are the following.

Shear thickening is only observed in a given concentration window, dependent upon the molecular weight of the polymer in solution. Below this window, only shear thinning is observed, as any structures formed are too small to affect either the rheological or the optical response of the solution. Within this window, structures form at low shear rates, increasing in size with increasing shear rate, and then begin to shrink near the critical shear rate where shear thickening begins. These structures are anisotropic and are one to two orders of magnitude smaller than micron size at maximum dimensions. The higher the shear rate, the more elongated they become, until ultimately they are reduced in size and aspect ratio by the increasing shear forces. For concentrations above this window, the structures continue to increase in size with increasing shear rate, eventually culminating in phase separation.

Perhaps the most interesting point, however, is that the model indicates that shear thickening is not at all related to phase separation, as asserted in the past, but is actually the antithesis of the same: shear thickening only appears when the associations prevalent in the solution are destroyed, not formed. One must first raise the solution concentration beyond the region where shear thickening occurs to see any phase separation whatsoever.

In conclusion, it seems fair to say that the hopeful prophecy of Kishbaugh, quoted at the beginning of the introduction, may have come to pass. Future work should focus on an understanding of the TCMM model in terms of more detailed molecular- and atomistic-based formulations, so that the internal physics of this structure formation may be evaluated.

REFERENCES

1. Kishbaugh, A. J. Ph.D. Dissertation, University of Illinois, 1992.
2. Kishbaugh, A. J.; McHugh, A. J. Rheol Acta 1993, 32, 9.
3. Kishbaugh, A. J.; McHugh, A. J. Rheol Acta 1993, 32, 115.
4. Beris, A. N.; Edwards, B. J. Thermodynamics of Flowing Systems; Oxford Univ. Press, New York, 1994.
5. Edwards, B. J.; Beris, A. N.; Mavrantzas, V. G. J Rheol 1996, 40, 917.

6. Layec-Raphalen, M.; Wolff, C. J Non-Newtonian Fluid Mech 1976, 1, 159.
7. Vrahopoulou, E. P.; McHugh, A. J. J Non-Newtonian Fluid Mech 1987, 25, 157.
8. Bird, R. B.; Curtiss, C. F.; Armstrong, R. C.; Hassager, O. Dynamics of Polymeric Fluids, 2nd ed.; John Wiley and Sons: New York, 1987; Vol. 2.
9. Peterlin, A. J Chem Phys 1960, 33, 1799.
10. Peterlin, A. Makromol Chem 1961, 45, 338.
11. Kishbaugh, A. J.; McHugh, A. J. J Non-Newtonian Fluid Mech 1990, 34, 181.
12. Grmela, M.; Carreau, P. J. J Non-Newtonian Fluid Mech 1987, 23, 271.
13. Wolff, C.; Silberberg, A.; Priel, Z.; Layec-Raphalen, M. N. Polymer 1979, 20, 281.
14. Wolff, C. Adv Colloid Interface Sci 1982, 17, 263.
15. Vrahopoulou, E. P.; McHugh, A. J. J Rheol 1987, 31, 371.
16. Vrahopoulou, E. P.; McHugh, A. J. Chem Eng Commun 1987, 57, 289.
17. Grmela, M.; Öttinger, H. C. Phys Rev E 1997, 56, 6620.
18. Öttinger, H. C.; Grmela, M. Phys Rev E 1997, 56, 6633.
19. Gurnee, E. F. J Appl Phys 1954, 25, 1232.
20. Kuhn, W.; Grün, F. Kolloid-Z 1942, 101, 248.
21. Copic, M. J Chem Phys 1957, 26, 1382.
22. Tsvetkov, V. N. Sov Phys Uspekhi 1964, 6, 639.
23. Ver Strate, G.; Philippoff, W. J Polym Sci, Polym Lett Ed 1974, 12, 267.
24. Rangel-Nafaile, C.; Metzner, A. B.; Wissbrun, K. F. Macromolecules 1984, 17, 1187.
25. Rietveld, J.; McHugh, A. J. J Polym Sci, Polym Lett Ed 1983, 21, 919.
26. Rietveld, J.; McHugh, A. J. J Polym Sci, Polym Phys Ed 1985, 23, 2339.
27. McHugh, A. J.; Blunk, R. H. Macromolecules 1986, 19, 1249.
28. Meeten, G. H. J Colloid Interface Sci 1980, 73, 38.
29. Meeten, G. H. J Colloid Interface Sci 1980, 74, 181.
30. Meeten, G. H. J Colloid Interface Sci 1981, 84, 235.
31. Meeten, G. H. J Colloid Interface Sci 1982, 87, 407.